Eurasian Journal of Physics and Functional Materials

Volume 8 | Number 2

Article 2

Pages: 71 - 78

2024

High-Temperature Thermally Stimulated Luminescence Of The Nacl And Nacl-Li Crystals

K. Shunkeyev
K. Zhubanov Aktobe Regional University, 34, A. Moldagulova Ave., 030000, Aktobe, Kazakhstan, sshynar.2021@gmail.com

Sh. Sagimbayeva
K. Zhubanov Aktobe Regional University, 34, A. Moldagulova Ave., 030000, Aktobe, Kazakhstan

L. Myasnikova
K. Zhubanov Aktobe Regional University, 34, A. Moldagulova Ave., 030000, Aktobe, Kazakhstan

A. Istlyaup
K. Zhubanov Aktobe Regional University, 34, A. Moldagulova Ave., 030000, Aktobe, Kazakhstan

A. Kenzhebayeva
K. Zhubanov Aktobe Regional University, 34, A. Moldagulova Ave., 030000, Aktobe, Kazakhstan

Recommended Citation

Shunkeyev, K.; Sagimbayeva, Sh.; Myasnikova, L.; Istlyaup, A.; and Kenzhebayeva, A. (2024) "High-Temperature Thermally Stimulated Luminescence Of The Nacl And Nacl-Li Crystals," *Eurasian Journal of Physics and Functional Materials*: Vol. 8: No. 2, Article 2.
DOI: https://doi.org/10.69912/2616-8537.1188

ORIGINAL STUDY

High-temperature Thermally Stimulated Luminescence of the NaCl and NaCl—Li Crystals

Kuanyshbek Shunkeyev, Shynar Sagimbayeva*, Lyudmila Myasnikova, Assel Istlyaup, Adelya Kenzhebayeva

K. Zhubanov Aktobe Regional University, 34, A. Moldagulova Ave., 030000, Aktobe, Kazakhstan

Abstract

This study delves into the investigation of the nature of high-temperature peaks observed in the thermally stimulated luminescence (TSL) of X-irradiated crystals of NaCl and NaCl—Li in a broad temperature range from 300 to 800 K. The research was conducted using the thermoluminescent dosimetric apparatus Harshaw 3500 (Thermo Fisher Scientific, USA).

The analysis revealed high-temperature TSL peaks categorized as Type I (360 ÷ 400K) and Type II (495 ÷ 620K), which are attributed to the thermal degradation of halogen defects, specifically $(Cl_3^-)_{aca}$- and $(Cl_n^-)_n$ -centers, respectively.

In NaCl—Li crystals, an experimental effect of increased light yield from Type II TSL peaks was observed. It intensifies with an increase in lithium concentration, and at lithium concentrations of 400 ppm intensity growth reaches two orders of magnitude higher ($10^5 \rightarrow 10^7$) compared to pure NaCl crystals.

The intense Type II TSL peaks (535 ÷ 570K) correlate with the increase in lithium concentration and the high-temperature incorporation of lithium into the NaCl—Li lattice. They serve as experimental evidence showcasing the efficiency of electron excitations decaying into radiation defects in the field of lithium ions under X-ray radiation exposure.

Keywords: Ionic crystal, High-temperature thermally stimulated luminescence, Crystal annealing, Light yield, Lithium impurity ion

1. Introduction

Currently, ionic crystals most commonly utilized as optical materials transparent in a broad spectrum [1—3], as scintillation [4—7] and thermoluminescent dosimeters [8,9] for detecting ionizing radiation in nuclear [8—10] and atomic [11,12] industries, medicine [13], ecology [14], and beyond.

What sets ionic crystals apart is their unique capacity to concurrently investigate luminescence emission (as scintillators) and the efficiency of radiation defect formation (as dosimeters), originating from the decay of e_s^0 self-trapped excitons (STEs) [2,3].

These two competing annihilation channels of STEs allow for the distinction of two groups of ionic crystals: scintillators and dosimeters.

Concurrently with the advancement of novel scintillators [4—7,15—17], there is an active endeavor to improve classical scintillators [4—7] based on ionic crystals (NaI, CsI).

Dosimeters based on LiF single crystals have found wide applications in dosimetric control of ionizing radiations in radiobiology [8—10], radiotherapy [12,13], personal dosimetry [12—14], as well as biological shielding against neutron radiation emitted by nuclear reactors [14—17], due to their tissue equivalence.

Because of the promising advancements in new technological applications (cryodetectors [8—10], nanotubes with hexagonal and octagonal cross-sections [18,19]), research on ionic crystals with the application of external perturbing factors has been revitalized: local deformation with the introduction of impurity ions [20—22], thermoelastic [23—25], uniaxial [26—29], and isotropic deformation [30—32].

A series of unique experiments [22,23,28] have been conducted the mechanism of converting absorbed

Received 28 March 2024; accepted 4 June 2024.
Available online 20 July 2024

* Corresponding author.
E-mail address: sshynar.2021@gmail.com (K. Shunkeyev).

https://doi.org/10.69912/2616-8537.1188

energy from ionizing particles into light. This process involves assembling electron-hole (*e-h*) pairs in the field of a light sodium ion in a KCl matrix.

Extensive research has been carried out in ionic crystals to study low-temperature (4.2 K→300 K) TSL peaks. These peaks are associated with determining the temperature at which self-localization, reorientation, delocalization, and recharge of primary radiation defects occur during STE's decay [2,3,33].

An established experimental result is worth noting: in the temperature range of 130K÷200K V_K-centers provide crucial information for studying TSL in alkali halide crystals. V_K-centers refer to self-trapped holes structured as $(X_2^-)_{aa}$, occupying two lattice anion sites with excess positive charge relative to the lattice [2,3,34−37]. The "X" symbol denotes a halide ion (e.g., Cl, Br, I). The self-localization of non-relaxed holes effectively occurs near vacancy defects (υ_c^-) and light cations (*Li, Na*), leading to the formation of various radiation defects in the V_K-family ($V_K(e_S^+)$, $V_F(e_S^+\upsilon_c^-)$, $V_{KA}(e_S^+Li)$ and $V_{KA}(e_S^+Na)$). The thermal destruction increases the probability of their recombination with F - centers, which is reflected in TSL peaks [2,3,34−38].

Understanding of the nature of high-temperature peaks in the TSL of ionic crystals, crucial indicators in ionizing radiation detection, remains incomplete due to two main factors, in our view. First of all, insufficient fundamental research owing to the unavailability of appropriate experimental setups for recording high-temperature TSL. Secondly, the non-systematic approaches to influencing the recombination luminescence of radiation defects, the concentration of light cation homologs (Li, Na), and high-temperature annealing.

Hence, this study aims to elucidate the nature of high-temperature peaks in the TSL of X-irradiated classical NaCl and NaCl−Li crystals over a broad temperature range of 300−800 K, until the complete fading of crystal color due to radiation defects. This investigation will be conducted using the thermoluminescent dosimetric setup Harshaw 3500 model by Thermo Fisher Scientific, USA.

2. Research objects and equipment

The NaCl and NaCl:Li crystals were grown at the Institute of Physics, University of Tartu, Estonia, using the Stockbarger method in a vacuum-sealed quartz ampoule following a stepwise preliminary purification process [38].

The purification algorithm for the crystals consists of the following sequential steps:

1. Prolonged vacuum drying of the powder-like raw material at 80−100 °C to remove oxygen-containing impurities (OCI). Absorption spectroscopy results indicate that the OCI impurity level is below 0.1 ppm, which is two orders of magnitude purer than the raw material.
2. Chlorine gas treatment of the NaCl melt to remove bromine impurities from the melt in gaseous form. This process involves substituting bromine ions with chlorine ions and removing bromine impurities from the NaCl melt in gaseous form. Absorption spectroscopy results show that the level of anionic and cationic homologous impurities is 1.5 ppm, which is two orders of magnitude purer than the raw material.
3. Multiple recrystallization, «zone melting» of the NaCl raw material melting based on the difference in incorporation coefficients (k) of ions from the melt into the solid solution. However, this method is not entirely effective for removing divalent impurities (e.g., Ca^{2+}) due to the proximity of k = 0.7. Therefore, the NaCl solution was purified by precipitating Ca^{2+} with barium added to the solution as carbonates ($BaCO_3$). Ion conductivity measurements show that the ultimate level of purification of NaCl from divalent metal ions is 0.5 ppm, which is three orders of magnitude purer than the raw material.

As a result of this comprehensive purification method, NaCl crystals with low impurity ion concentrations of 0.1−1.5 ppm were obtained.

The NaCl:Li crystals were grown from purified NaCl raw material (as described above) with the addition of pre-dried LiCl powders. The incorporated concentration of LiCl powder into the charge (quartz ampoule) containing NaCl powder is within the range of 500−2000 ppm. The lithium ion concentration in the NaCl:Li single crystals, considering the lithium incorporation coefficient (k = 0.2) into the NaCl crystal lattice, was within the range of 100−400 ppm, consistent with flame photometry data.

In our practice, to avoid contamination, the zone purification and crystal growth using the Stockbarger method were combined by varying the lifting speed of the quartz ampoule in the final stage of zone melting to a slower speed of 2−4 mm/hour.

The investigation encompassed natural NaCl crystals (Halite) grown under natural conditions at the “Sol-Iletsk” deposit. Unlike crystals synthesized from melts (above 800 °C), the natural growth of halite at low temperatures (5−10 °C) exhibits commendable structure and purity, devoid of divalent impurities. However, sensitive luminescent methods detected the presence of lithium ions in natural NaCl crystals at approximately 100−200 ppm, which becomes evident after tempering the crystals.

The tempering process for the studied crystals was conducted using the "Programix TX 25″ electric muffle furnace manufactured by "Ugin-Dentaire" company. This involved a programmed tempering regime, including heating at a rate of 15 °C/min to the specified temperature (650−700 °C), holding for 15 minutes, and rapid cooling on a quartz substrate to room temperature in ambient air [22−24].

The research focused on NaCl (zone-purified) and NaCl−Li (100−400 ppm of Li) crystals, allowing for variations in matrix purity, which is crucial for interpreting the high-temperature peaks of thermoluminescence in these crystals. In NaCl (Halite) and NaCl (Harshaw) crystals, the concentrations of lithium are approximately 500 ppm and 100 ppm, respectively.

The presence of uncontrolled impurities of light cation homologs (Li) in the lattice with an ionic radius significantly smaller than that of the host cation in the matrix (e.g., NaCl−Li), was activated through tempering, a proven method for stabilizing the crystalline system [22,23,34].

Ionizing radiation was provided by the bremsstrahlung from the RUP-120 setup with a W-antikathode, operating at 3 mA and 100 kV.

The high-temperature thermally stimulated luminescence (TSL) of crystals was measured at a constant rate of $\beta = 5.0$ K/s in a broad temperature range (300 ÷ 850 K) using the Harshaw Model 3500 thermoluminescent dosimetry system. Experiment control was facilitated through a computer connected to the Harshaw 3500 system via an RS 232 port and equipped with WinREMS software (Windows Radiation Evaluation and Management System). WinREMS managed various functions of the Harshaw 3500 system, including loading and storing operational parameters such as temperature-time profiles (TTP), ratio correction factors (RCF), and element correction coefficient (ESC). Additionally, it facilitated conversions to different dosimetric measurement units (roentgen, gray, rad, becquerel, sievert).

The digital data extracted from the WinREMS-controlled software delineates the TSL curves of crystals and is exported in (.txt) format for subsequent analysis using Origin Pro software. This analytical tool enables the creation of graphical representations illustrating the intensity of TSL peaks relative to the heating temperature applied to the samples.

The comparison of the TSL light yield from the examined crystals meticulously followed their dimensions and exposure duration during X-ray irradiation. This precision is crucial as the cumulative recombination luminescence from radiation defects directly correlates with the dose of ionizing radiation received within a specified timeframe.

3. Experimental results

The recombination luminescence of radiation defects, forming the basis of TSL, can be categorized into two types: electron recombination luminescence involves the recombination of free electrons with self-trapped holes, while hole recombination luminescence entails the recombination of non-relaxed holes with localized electrons.

3.1. The effect of light lithium cation on the formation of high-temperature TSL peaks in the NaCl crystal matrix

In ionic crystals above room temperature, stable radiation defects exist in the form of complementary pairs $V_2 = (X_3^-)_{aca}$- and $F(\upsilon_a^+ e^-)$-centers [2,3,35−38]. Thermal annealing of these centers coincides with luminescence in the temperature range 380 ÷ 400K, following this scheme:

$$V_2 + T, K \rightarrow (V_2)^* \rightarrow V_F + H.....F \rightarrow e_S^+ \upsilon_c^- + e^- \upsilon_a^+ \rightarrow I_{TSL}(380 \div 400K)$$

As a consequence of the thermal delocalization of V_2-centers, their dissociation products are mobile V_F- and H-centers, as indicated in the reaction mentioned above. These centers carry positive charges relative to the lattice and exhibit a high probability of recombining with immobile F-centers. This process results in the formation of a TSL peak with a maximum observed the temperature range from 380 ÷ 400K. The shift in the TSL peak's maximum is attributed to the concentrations of V_2-center dissociation products and the presence of luminescent electron-hole pairs surrounded by anion (υ_a^+) and cation (υ_c^-) vacancies, which are integral components of V_F- and F-centers.

Extensive studies have delved into the processes of formation and dissociation of X_3-centers associated with high-temperature TSL peaks in alkali halide crystals [2,3,34−38]. However, there remains a notable absence of systematic study of TSL peaks exceeding 400 K, concerning crystal purity and quenching temperatures, factors that disrupt the aggregation of halogens and electronic radiation defects in alkali halide crystals.

Figs. 1−3 depict the outcomes of recording high-temperature TSL peaks in zone-purified NaCl crystals (Fig. 1), which serve as a purity reference, as well as in NaCl−Li crystals with increasing lithium concentrations up to 100 ppm (Fig. 2) and 400 ppm (Fig. 3).

Crystal irradiation to accumulate radiation defects utilized X-rays from bremsstrahlung, ensuring penetration through the entire crystal thickness, in contrast to characteristic radiation emitted from the RUP-120 setup (W-antikathode, operating at 3 mA and 100 kV)

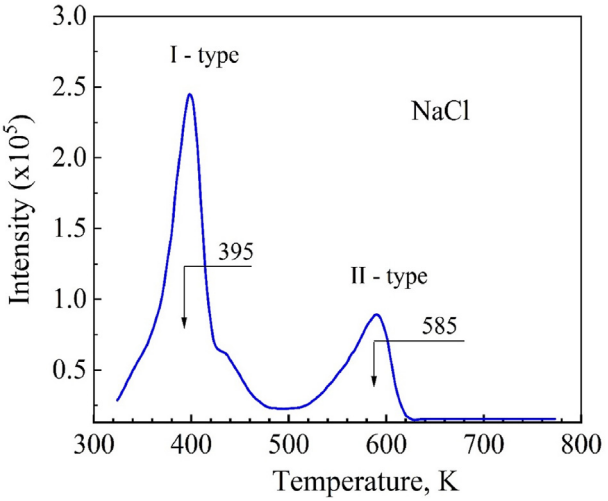

Fig. 1. Integral thermally stimulated luminescence of a zone-purified NaCl crystal.

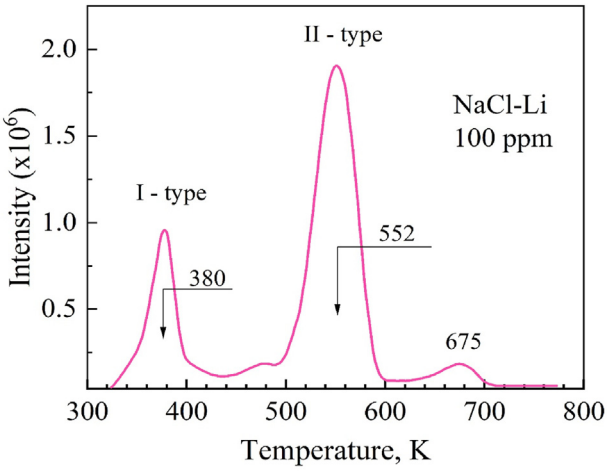

Fig. 2. Integral thermally stimulated luminescence of NaCl–Li crystal (100 ppm).

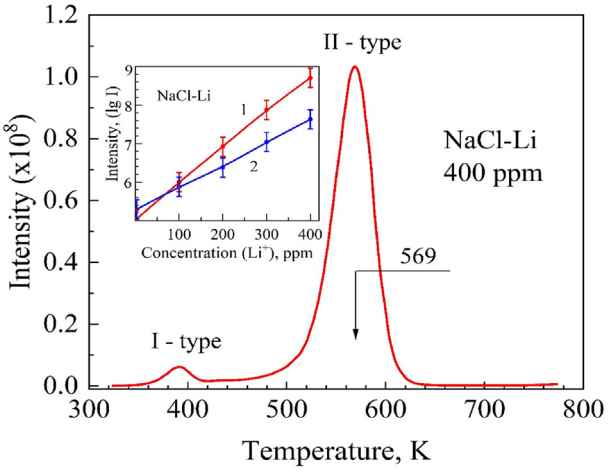

Fig. 3. Integral TSL of NaCl–Li (400 ppm) crystal. Inset: Dependence of the TSL peaks' intensity at 569K (1) and at 390K (2) on the concentration of lithium in the NaCl–Li matrix.

under uniform dosage exposure ($1 \cdot 10^{-3}$ Gy) at room temperature.

From Fig. 1, it can be inferred that the predominant TSL peak is the well-known peak with a maximum at 395 K (V_2-centers), as discussed in detail above. Additionally, there are weak and unresolved peaks in the temperature range of 520 ÷ 620K, with a maximum at 585 K. It is evident that the emission spectrum consists of several competing bands, with intensities 2.5 times weaker than that of the V_2-centers. For convenience, we will denote them as high-temperature TSL peaks of Type I (380 ÷ 400K) and Type II (520 ÷ 620K).

As the concentration of lithium in the crystals increased, the picture changed dramatically, as shown in Figs. 2 and 3, in favor of the Type II TSL peak.

In the NaCl–Li crystals (100 ppm), a previously undetected, entirely new dominant TSL peak emerges. This peak exhibits a maximum at 552 K (Type II), showing twice the intensity of the Type I TSL peak (Fig. 2) and 22.5 times the intensity of the Type II TSL peak in NaCl crystals (refer to Table 1, second row in the last column).

The half-width of the 552 K TSL peak in the NaCl–Li (100 ppm) crystal is approximately 50 K, which is sufficiently wide for an elementary TSL peak, indicating a composite band likely composed of at least two luminescence centers. Additionally, less intense TSL peaks with maxima at 480K and 675K are also observed.

The main effect observed in this experiment is that the appearance of the new intense Type II TSL peak of (552 K) is initiated by a small concentration of lithium (100 ppm) doped into the NaCl crystalline matrix. This implies that the presence of lithium in the NaCl lattice leads to a sharp increase in the concentration of radiation-induced defects, created from non-radiative decay of electronic excitations, most likely electron-hole (e-h) pairs, as the output of radiation defect formation, unlike excitons, increases with temperature. Each TSL peak characterizes the maximum temperature of recombination of oppositely charged delocalized radiation-induced defects, and the intensity of the TSL peak indicates an increased concentration of recombining radiation-induced defects (see also Fig. 2).

For the purpose of validating the effect of lithium on the heightened intensity of the newly identified Type II (I_{II}) TSL peak, our primary focus centers on examining the intensity dependence on lithium concentration (C_{Li}) within NaCl–Li crystals.

With further increases in the lithium concentration in NaCl–Li crystals, the intensity of the Type II TSL peak experiences a substantial increase, reaching an amplification of 8750-fold compared to zone-purified NaCl crystals at 400 ppm (refer to Table 1, fifth row of the final column). The dynamics of the intensity dependence $I_{II} \sim f(C_{Li})$ are depicted in the inset of Fig. 3,

Table 1. Dependency of the intensity of high-temperature TSL peaks on lithium concentration in the NaCl crystalline matrix.

NO	Crystals	Type I TSL peak	Type II TSL peak	The ratio of peaks TSL (I_{II}/I_I)	Increase in Type II TSL peak intensity with increasing lithium concentration
1	NaCl (reference)	$2.5 \cdot 10^5$	$0.8 \cdot 10^5$	0.32	1
2	NaCl—Li (100 ppm)	$1.0 \cdot 10^6$	$1.8 \cdot 10^6$	1.8	22.5
3	NaCl—Li (200 ppm)	$4.0 \cdot 10^6$	$9.0 \cdot 10^6$	2.3	112.5
4	NaCl—Li (300 ppm)	$1.0 \cdot 10^7$	$7.9 \cdot 10^7$	7.9	987.5
5	NaCl—Li (400 ppm)	$6.5 \cdot 10^7$	$7.0 \cdot 10^8$	11	8750

derived from numerous experimental data points detailed in Table 1, with an error margin not exceeding 10%.

In the NaCl—Li crystal, as indicated in the inset of Fig. 3 and Table 1 (by comparing across rows 1—5 of Column 1), the augmentation of the Type II TSL peak's intensity is accompanied by a concurrent increase in the intensity of the Type I TSL peak. This elevation is attributed to the thermal decomposition of $V_2 = (Cl_3^-)_{aca}$-centers. The dynamics of the intensified Type I TSL peak (380 ÷ 400K) with increasing lithium concentration in NaCl—Li crystals reaffirms that the light impurity cation lithium, with an ionic radius (0.68 Å) smaller than that of the native sodium lattice cation (0.98 Å), facilitates the efficient formation of radiation defects. These defects, stabilized by the extensively studied $V_2 = (Cl_3^-)_{aca}$-centers, represent the culmination of their stabilization process.

In essence, this experimental evidence conclusively demonstrates that the emergence of high-temperature Type II TSL peaks in the NaCl matrix is directly attributed to the presence of lithium ions. Firstly, lithium stimulates the efficient generation of halogen radiation defects, and secondly, it serves as a diagnostic tool to capture the dissociation products of thermally disintegrated halogen formations and electronic centers, manifested as the recombination luminescence of electron-hole pairs.

3.2. Thermal activation of lithium incorporation into the NaCl—Li crystal lattice

Experimental studies of absorption and luminescence spectroscopy [22,23] have revealed the phenomenon of instability within the adjacent crystalline system of KCl—Na. The system is doped with sodium, an ion with an ionic radius (0.68 Å) smaller than that of potassium (1.33 Å), i.e. the cation of the main lattice.

The coefficient (k) of dopant incorporation into the crystal lattice (Column 1), which correlates with the ratio of cationic radii between the main lattice and the dopants (Column 2), allows us to anticipate the instability dynamics in ionic crystals. This particularly applies to NaCl:Li, KCl:Na, and KCl:Li crystals that incorporate light homologous cations as dopants (refer to Table 2). The dopant cations (Li, Na) display remarkably low incorporation coefficients: NaCl:Li (k = 0.2), KCl:Na (k = 0.3), and KCl:Li (k = 0.02); the phenomenon presumably leads to the emergence of an instability effect in the crystalline system.

The instability effect in the KCl—Na system stems from the fact that, at room temperature, the mobility of cationic vacancies has a positive value, unlike the anionic vacancies in the lattice. As a result, over extended storage periods (more than 3 months), the dopant sodium ion has a high probability of shifting from its regular cationic lattice site.

In simpler terms, the process of displacing the dopant sodium ion from its designated lattice site leads to the “self-cleansing” of the KCl matrix from sodium. The measuring equipment does not detect (or records weak signals) any signs of sodium presence in the cationic lattice site. A similar scenario is observed for “decomposed” NaCl—LiCl crystals with a relatively high lithium concentration (400 ppm), as depicted in Fig. 4. They previously exhibited an intense signal (over $1 \cdot 10^8$ pulses in Fig. 3) at the peak of the Type II TSL (569K).

Upon observing the TSL curves (Fig. 4), it initially appears as though we are dealing with a pure crystal, as the TSL intensity of NaCl—LiCl (Fig. 3) is “damped” by a factor of 1000 ($10^8 \rightarrow 10^5$), almost reaching the level of the zone-purified NaCl crystal (Fig. 1). Notably, the NaCl—LiCl crystals (400 ppm) in Figs. 3 and 4 represent the same crystal, but the TSL in Fig. 4 belongs to the decomposed NaCl—LiCl crystal (400 ppm). The TSL curves of the NaCl—LiCl crystal (400 ppm) are more intense compared to the zone-purified NaCl crystal (Fig. 1) and exhibit distinct peaks at 362K, 440K, 472K, and 544K, with the first and last ones

Table 2. The coefficients of impurity homologue cations incorporation into the NaCl and KCl crystal matrices [22,23].

NO	Crystals	Ratios of the radii of main lattice cations and impurity cations	The coefficient (k) of an impurity incorporation into the main lattice
1.	NaCl—LiCl	[r(Na)/r(Li)] = 1.44	0.2
2.	KCl—NaCl	[r(K)/r(Na)] = 1.35	0.3
3.	KCl—LiCl	[r(K)/r(Li)] = 1.95	0.02
4.	NaCl—$CaCl_2$	[r(Na)/r(Ca)] = 1.44	0.9

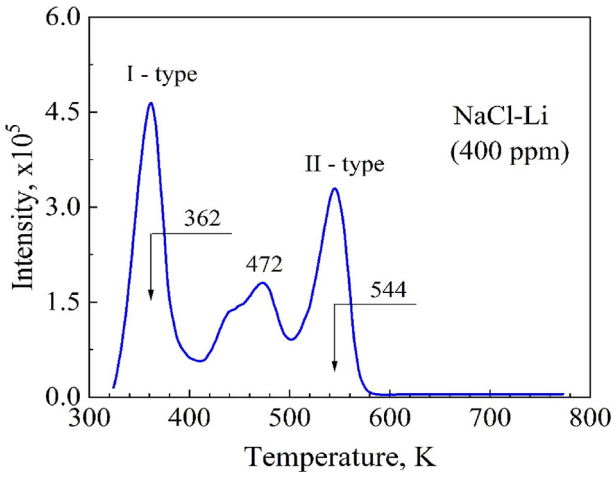

Fig. 4. Thermally stimulated luminescence of a decomposed NaCl—Li crystal (400 ppm).

corresponding to TSL peaks of Types I and II, respectively.

The ratio of Type I and Type II TSL intensities in the zone-purified NaCl crystal was 0.32 (refer to Fig. 1 and Table 1, first row penultimate column). For NaCl—LiCl (400 ppm), it was 0.7 (Fig. 4), indicating the presence of lithium traces in the cationic lattice site.

The crystal underwent intermediate annealing by heating it to 500 °C at a rate of 15 °C per minute and maintaining this temperature for 15 minutes. Subsequent rapid cooling to room temperature on a quartz substrate significantly altered the overall outcome, as depicted in Fig. 5.

It is important to emphasize that the X-ray radiation doses were consistently maintained at $(1 \div 5)\cdot 10^{-3}$ Gy in all experiments conducted for luminescence registration on the crystals.

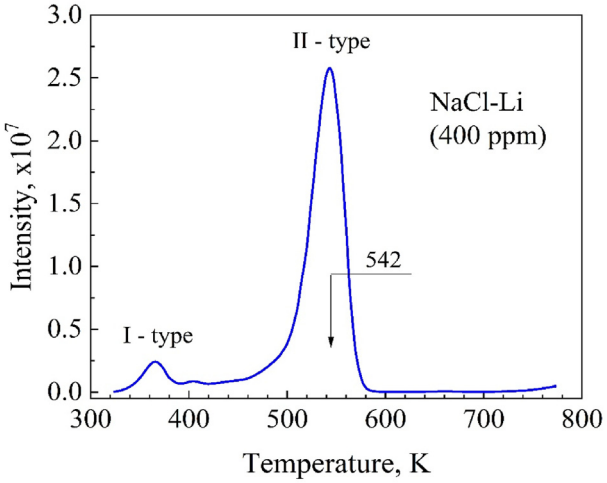

Fig. 5. Thermally stimulated luminescence of a decomposed NaCl—Li crystal (400 ppm) after annealing at 500 °C. The same crystal from Fig. 4.

Fig. 5 reveals that the annealed (500 °C) NaCl—Li (400 ppm) crystal shows an increase in the intensities of both Type I and Type II TSL peaks, approximately two orders of magnitude higher ($10^5 \rightarrow 10^7$). The intensities are brought closer to those observed in the unaltered crystal (Fig. 3), contrasting with the decomposed crystal (Fig. 4). Furthermore, the intensity ratios have been restored, favoring the Type II TSL peak with a maximum at 542K. Aside from the shift of the maximum, asymmetry in the full width at half maximum is evident, indicating non-elementary nature of the peaks. The temperature shift of the Type II TSL peak (542K÷569K) likely stems from various competing factors influencing the mechanism behind the high-temperature TSL peak formation in the NaCl—Li crystal matrix. Among these factors, the presence of small lithium ions in the lattice, with an ionic radius (0.68 Å) smaller than that of sodium (0.98 Å), attracts the anionic environment. It contributes to the localization of mobile radiation defects in the form of recombination luminescence stimulated by heating the NaCl—Li crystal to high temperatures (500K ÷ 600K).

Subsequent annealing of the NaCl—Li (400 ppm) crystal to 650 °C revealed (Fig. 6) an intensity increase surpassing 10^9, exceeding the intensity of the unannealed, freshly grown crystal by more than an order of magnitude (as seen in Fig. 3). Additionally, a doublet structure of the high-temperature Type II TSL peak was observed with maxima at 539K and 563K.

The inset of Fig. 6 presents the dependence of Type II TSL intensity on annealing temperature ($I \sim f(t)$) for decomposed NaCl—Li crystals (400 ppm), covering a range from 100 °C to 720 °C. The numerical values are provided in Table 3.

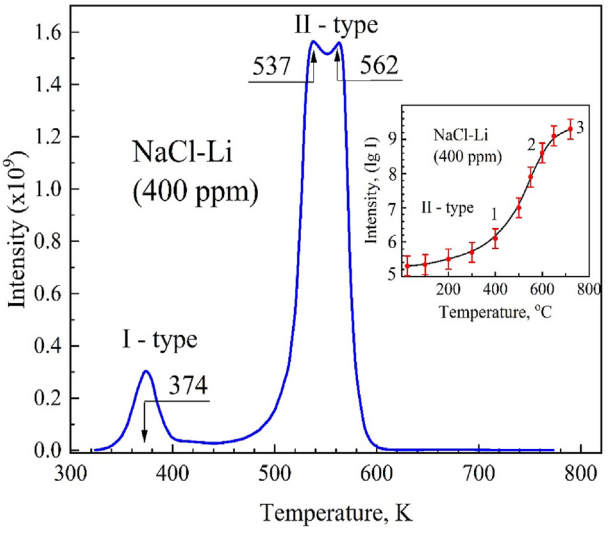

Fig. 6. Thermally stimulated luminescence of a decomposed NaCl—Li crystal (400 ppm) after annealing at 650 °C. The same crystal from Fig. 4.

Table 3. The dependence of the intensity of the Type II TSL peak on the annealing temperature of the decomposed NaCl−Li (400 ppm) crystal.

No	The annealing temperature (t, °C)	The intensity of the Type II TSL peak	The increase in intensity of the Type II TSL peak
1.	27	$3.0 \cdot 10^5$	1
2.	100	$3.2 \cdot 10^5$	1.06
3.	200	$5.0 \cdot 10^5$	1.6
4.	300	$7.0 \cdot 10^5$	2.3
5.	400	$1.0 \cdot 10^6$	3.3
6.	460	$5.0 \cdot 10^6$	16.6
7.	500	$9.0 \cdot 10^6$	30
8.	560	$8.5 \cdot 10^7$	283
9.	600	$6.0 \cdot 10^8$	2000
10.	650	$1.0 \cdot 10^9$	3333
11.	720	$2.5 \cdot 10^9$	8333

According to the data in Table 3 and the $I \sim f(t)$ dependence, annealing the crystals in the temperature range from 100 °C to 400 °C results in a nonlinear increase in the intensity of the Type II TSL peak with a growth of only 3.3 times at 400 °C (point 1 in the inset of Fig. 6). In the temperature range from 400 °C to 600 °C, the intensity of the Type II TSL peak increases by 16.6 and 2000 times, respectively (Table 3), exhibiting a linear trend (points 1 → 2 in the inset of Fig. 6). At higher annealing temperatures (up to 720 °C), saturation of the $I \sim f(T)$ dependence is observed (2 → 3).

Under the conditions of high-temperature annealing at 600 °C ÷ 720 °C, the mobility of interstitial lithium ions appears to increase, which facilitates the incorporation of lithium into the cation site of the lattice [22,23]. It possibly leads to the formation of vacancy defects, as evidenced by the enhanced efficiency of radiation-induced Type I TSL peak formation (380 ÷ 400K, Fig. 6), which includes divacancies ($v_a^+ v_c^-$).

Comparative analysis of Table 1 data (fifth row, last column − 8750 impulses) and Table 3 data (eleventh row, last column − 8333 impulses) indicates that the lattice of the decomposed NaCl−Li (400 ppm) crystal has almost completely regained its structure (95%), as their peak intensities are very close − 8750 and 8333 impulses.

It can be hypothesized that during high-temperature annealing (up to 600 °C), light lithium ions are released from halogen clusters and reintegrated into the regular cationic sites of the NaCl−Li (400 ppm) crystal lattice.

The decomposition of the TSL peaks into elementary components (dashed lines in Fig. 6) reveals an anomalously narrow half-width TCJI ($\Delta_1 = 23$ K, $\Delta_2 = 39$ K, $\Delta_3 = 29$ K), which is atypical for high-temperature TSL peaks representing deep traps with high activation energy.

In the 500 ÷ 600K temperature range, there is presumably an « explosive » dissociation of complex $(Cl_n^-)_n$ halogen formations much larger than the $(Cl_3^-)_{aca}$-centers (380 ÷ 400 K). This results in the formation of a stream of unrelaxed "hot" holes and electrons (similar to X-ray excitation), which recombine in the field of small lithium, creating a potential well for their assembly with maximum luminescence output. Such a mechanism of recombination luminescence may explain the narrow TSL half-width. The doublet of Type II TSL bands with peaks at 537 K and 562 K probably attributed to the non-central position of the lithium ion in the NaCl crystal's cationic sublattice due to the difference in ionic radii of the cations (Li, Na).

4. Conclusion

Based on the experimental results obtained during the investigation of high-temperature TSL peaks in monocrystalline NaCl matrices following room temperature X-ray radiation exposure, it is important to discuss the key patterns and characteristics as follows.

In ultra-pure NaCl crystals, the dominant TSL peak at 400K corresponds to the intrinsic lattice radiation defect, the $V_2 = (Cl_3^-)_{aca}$- center, formed through the interaction of mobile halide atoms [2,3,35−37], designated as Type I TSL peak according to our notation. In ultra-pure NaCl crystals, above the temperature of $V_2 = (Cl_3^-)_{aca}$- center delocalization, unresolved and weak intensity Type II TSL peaks are observed (Fig. 1), indicating a low proportion of uncontrolled impurities (0.05−0.1 ppm) after comprehensive purification (see also section 2). This is confirmed by the intensive growth of Type II TSL peaks with increasing lithium concentration $I_{II} \sim f(C_{Li})$ in NaCl−Li crystals (see insert in Fig. 3). At a lithium concentration of 400 ppm, the increase in the intensity of the Type II TSL peak in NaCl−Li crystals compared to zone-refined NaCl crystals is 8750 times (Table 1, see the fifthth row of the last column). More effective incorporation of lithium into the NaCl lattice was achieved by high-temperature annealing of crystals, the results of which are shown in Fig. 6 and Table 3.

Hence, it can be confidently asserted that the Type II TSL peaks at high temperatures correlate with the breakdown of more heat-resistant halogen structures (up to 570 K), involving lithium impurity ions within the NaCl matrix.

Using the NaCl−Li crystal as an example, it can be hypothesized that the high-temperature TSL peaks, which form the basis of dosimetric detectors, are highly sensitive to the presence of light homologous cation impurities. Therefore, the newfound results concerning the amplification of light yield from recombination luminescence of radiation defects represent an essential parameter in the advancement of contemporary dosimetric crystals.

Conflicts of interest

The authors declare no conflicts of interest.

Acknowledgments

The authors express their sincere gratitude to Ministry of Science and Higher Education the Republic of Kazakhstan for providing a research project of grant funding.

The research was conducted as part of a grant project funded by the Science Committee of the Ministry of Science and Higher Education the Republic of Kazakhstan (Grant No. AP23488688).

References

[1] N. Itoh, A.M. Stoneham, Materials Modification by Electronic Excitation, Cambridge University Press, Cambridge, 2001, p. 538.
[2] Ch. Lushchik, In: R. Johnson, A. Orlov (Eds.), Physics of Radiation Effects, 1986, p. 736. North-Holland, Amsterdam.
[3] K. Song, R. Williams, Self-Trapped Excitons, second ed., Springer, Berlin, 1996, p. 410.
[4] V. Kumar, Z. Luo, Review on X-ray excited emission decay dynamics in inorganic scintillator materials, Photonics 8 (71) (2021) 1–27.
[5] Y. Takizawa, K. Kamada, M. Yoshino, J.K. Kim, N. Kutsuzawa, A. Yamaji, S. Kurosawa, Y. Yokota, H. Sato, S. Toyoda, Y. Ohashi, T. Hanada, V. Kochurikhin, A. Yoshikawa, Growth of thallium-doped CsI/CsCl/KCl eutectics and their scintillation properties, Opt. Mater. X 15 (2022) 100159.
[6] Y. Rodriguez-Lazcano, V. Correcher, J. Garcia-Guinea, Radiat. Phys. Chem. 81 (2012) 126–130.
[7] M.K. Muhamad Azim, S.F. Abdul Sani, E. Daar, M.U. Khandaker, K.S. Almugren, F.H. Akkallas, D.A. Bradley, Radiat. Phys. Chem. 176 (2020) 108964.
[8] Ch.J. Hailey, W.W. Craig, F.A. Harrison, J. Hong, K. Mori, J. Koglin, H.T. Yu, K.P. Ziock, Nucl. Instrum. Methods B. 214 (2004) 122, https://doi.org/10.1016/j.nimb.2003.08.004.
[9] F. Froborg, A. Duffy, J. Phys. G Nucl. Part. Phys. 47 (2020) 49, https://doi.org/10.1088/1361-6471/ab8e93.
[10] G. Adhikari, P. Adhikari, E. Barbosa de Souza, et al., Phys. Rev. Lett. 123 (2019) 031302, https://doi.org/10.1103/PhysRevLett.123.031302.
[11] M. Konopka, P. Bilski, B. Obryk, B. Marczewska, P. Olko, M. Klosowski, W. Gieszczyk, Luminescence dosimetry: review of methods, detectors and their applications, Nonlinear Opt. Quant. Opt. 48 (2017) 133–146.
[12] L.A.R. Da Rosa, S.C. Cardoso, L.T. Campos, V.G.L. Alves, D.V.S. Batista, A. Facure, Percentage depth dose evaluation in heterogeneous media using thermoluminescent dosimetry, J. Appl. Clin. Med. Phys. 11 (1) (2010) 117–127.
[13] M. Khoshakhlagh, J. Islamian, S. Abedi, B. Mahmoudian, Development of scintillators in nuclear medicine, World J. Nucl. Med. 14 (3) (2015) 156–159.
[14] K. Watanabe, Y. Kawabata, A. Yamazaki, A. Uritani, T. Iguchi, K. Fukuda, T. Yanagida, Development of an optical fiber type detector using a Eu:LiCaAlF$_6$ scintillator for neutron monitoring in boron neutron capture therapy, Nucl. Instrum. Methods Phys. Res. Sect. A Accel. Spectrom. Detect. Assoc. Equip. 802 (2015) 1–4.
[15] K. Miyazaki, D. Nakauchi, T. Kato, N. Kawaguchi, T. Yanagida, Suppression of afterglow in RbI:Tl scintillator by co-doping, J. Mater. Sci. Mater. Electron. 34 (13) (2023) 1082.
[16] K. Miyazaki, D. Nakauchi, T. Kato, N. Kawaguchi, T. Yanagida, Development of Tl-doped KI single crystal scintillators, Radiat. Phys. Chem. 207 (2023) 110820.
[17] K. Miyazaki, D. Nakauchi, T. Kato, N. Kawaguchi, T. Yanagida, Tl-concentration dependence of photoluminescenceand scintillation properties in Tl-doped RbI single crystals, J. Mater. Sci. Mater. Electron. 33 (2022) 22162–22168.
[18] D.M. Sergeyev, K.S. Shunkeyev, Russ. Phys. J. 60 (2018) 1938, https://doi.org/10.1007/s11182-018-1306-9.
[19] D.M. Sergeyev, K.S. Shunkeyev, N. Zhanturina, S.K. Shunkeyev, 49 (1), in: IOP Conference Series: Materials Science and Engineering, 2013 012049, https://doi.org/10.1088/1757-899X/49/1/012049.
[20] K. Miyazaki, D. Nakauchi, T. Kato, N. Kawaguchi, T. Yanagida, Radiat. Phys. Chem. 207 (2023) 110820, https://doi.org/10.1016/j.radphyschem.2023.110820.
[21] K. Miyazaki, D. Nakauchi, T. Kato, N. Kawaguchi, T. Yanagida, J. Mater. Sci. Mater. Electron. 33 (28) (2022) 22162, https://doi.org/10.1007/s10854-022-08996-y.
[22] K. Shunkeyev, A. Tilep, Sh. Sagimbayeva, A. Lushchik, Z. Ubaev, L. Myasnikova, N. Zhanturina, Z. Aimaganbetova, Nucl. Instrum. Methods B 528 (2022) 20, https://doi.org/10.1016/j.nimb.2022.08.002.
[23] K. Shunkeyev, A. Tilep, Sh. Sagimbayeva, Z. Ubaev, A. Lushchik, Crystals 13 (2) (2023) 364, https://doi.org/10.3390/cryst13020364.
[24] L. Myasnikova, K. Shunkeyev, N. Zhanturina, Z. Ubaev, A. Barmina, Sh. Sagimbaeva, Z. Aimaganbetova, Nucl. Instrum. Methods B. 464 (2020) 95, https://doi.org/10.1016/j.nimb.2019.12.014.
[25] K. Shunkeyev, D. Sergeyev, W. Drozdowski, K. Brylev, L. Myasnikova, A. Barmina, Sh. Sagimbaeva, Z. Aimaganbetova, J. Phys. Conf. 830 (1) (2017) 012139.
[26] K. Shunkeyev, A. Lushchik, L. Myasnikova, Sh. Sagimbaeva, Zh. Ubaev, Z. Aimaganbetova, Low Temp. Phys. 45 (2019) 1127, https://doi.org/10.1063/1.5125992.(EX RbI).
[27] K. Shunkeyev, A. Lushchik, Sh. Sagimbayeva, Z. Ubaev, A. Tilep, L. Myasnikova, Nucl. Instrum. Methods B 547 (2024) 165194, https://doi.org/10.1016/j.nimb.2023.165194.
[28] K. Shunkeyev, Z. Aimaganbetova, L. Myasnikova, A. Maratova, Z. Ubaev, Nucl. Instrum. Methods B 509 (2021) 7, https://doi.org/10.1016/j.nimb.2021.10.010.
[29] Y. Kohzuki, T. Ohgaku, J. Lumin. 253 (2023) 119469, https://doi.org/10.1016/j.jlumin.2022.119469.
[30] M. Ramirez, L. Bausa, S.W. Biernacki, A. Kaminska, A. Suchocki, M. Grinberg, Phys. Rev. B 72 (2005) 224104, https://doi.org/10.1103/PhysRevB.72.224104.
[31] M. Grinberg, J. Lumin. 131 (2011) 433, https://doi.org/10.1016/j.jlumin.2010.10.043.
[32] S. Mahlik, M. Malinowski, M. Grinberg, Opt. Mater. 33 (2011) 152, https://doi.org/10.1016/j.optmat.2011.02.001.
[33] K. Shunkeyev, L. Myasnikova, A. Barmina, Z. Aimaganbetova, D.M. Sergeyev, J. Phys. Conf. 830 (1) (2017) 012138.
[34] K. Shunkeyev, Zh. Ubaev, A. Lushchik, L. Myasnikova, Radiation defects in **NaCl** matrix with reduced lattice symmetry caused by light cation doping and elastic uniaxial deformation, Lith. J. Phys. 61 (3) (2021) 151–160, https://doi.org/10.3952/physics.v61i3.4514.
[35] A. Elango, T. Nurakhmetov, Phys. Stat. Sol. (B) 78 (2) (1976) 529, https://doi.org/10.1002/pssb.2220780211.
[36] A. Lushchik, Ch. Lushchik, N. Lushchik, A. Frorip, O. Nikiforova, Phys. Status Solidi B 168 (1991) 413, https://doi.org/10.1002/pssb.2221680204.
[37] A. Lushchik, I. Kudryavtseva, Ch. Lushchik, E. Vasil'chenko, M. Kirm, I. Martinson, Phys. Rev. B 52 (14) (1995) 10069, https://doi.org/10.1103/PhysRevB.52.10069.
[38] Ch. Lushchik, A. Lushchik, Decay of Electronic Excitations with Defect Formation in Solids, Nauka, Moscow, 1989, p. 263 (in Russian).